



# Synthesis of Core-Shell Magnetic Supramolecular Nanocatalysts based on Amino-Functionalized Calix[4]arenes for the Synthesis of 4*H*-Chromenes by Ultrasonic Waves

Reza Eivazzadeh-Keihan,<sup>[a]</sup> Ehsan Bahojb Noruzi,<sup>[b]</sup> Fateme Radinekiyan,<sup>[a]</sup> Milad Salimi Bani,<sup>[c]</sup> Ali Maleki,<sup>\*[a]</sup> Behrouz Shaabani,<sup>\*[b]</sup> and Mohammad Haghpanahi<sup>\*[c]</sup>

One of the most common phenol-formaldehyde cyclic oligomers from hydroxyalkylation reactions that exhibit supramolecular chemistry are calixarenes. These macrocyclic compounds are qualified to act as synthetic catalysts due to their specific features including being able to form host-guest complexes, having unique structural scaffolds and their relative ease of chemical modifications with a variety of functions on

their upper rim and lower rim. Here, a functional magnetic nanocatalyst was designed and synthesized by using a synthetic amino-functionalized calix[4]arene. Its catalytic activity was evaluated in a one-pot synthesis of 2-amino-4*H*-chromene derivatives. Besides, this novel magnetic nanocatalyst was characterized by spectroscopic and analytical techniques such as FT-IR, EDX, FE-SEM, TEM VSM, XRD analysis.

## 1. Introduction

A supramolecule is a complex of several molecules that aggregate by noncovalent binding interactions such as hydrogen bonding, cation- $\pi$ , anion- $\pi$  and,  $\pi$ - $\pi$  interactions.<sup>[1]</sup> Supramolecules are often held together and are highly dynamic compounds. As noncovalent interactions are important in catalysis chemistry, one important aspects of supramolecular chemistry is designing new catalysts with unique properties. Supramolecular catalysts accelerate reactions by (i) increasing the effective local concentration of the reactants via encapsulation,<sup>[2]</sup> (ii) utilizing intermolecular forces to guide substrates towards the transition state, (iii) stabilizing the transition state of the reaction and reducing activation energy and (iv) approaching host and guest molecules together.<sup>[3]</sup> One of the prominent classes of supramolecules are calixarenes


(CAs) which are derived from the condensation reaction of phenols with formaldehyde.<sup>[4]</sup> CAs have several special features:<sup>[5]</sup> notably, they are able to form host-guest complexes and they can host a large variety of functions on the upper rim and lower rim. These features have qualified them to be good candidates to act as organic chelating ligand,<sup>[6]</sup> drug carrier<sup>[7]</sup> and synthetic catalysts. There are lots of example for calixarene catalytic activities. Magnetically functionalized CAs efficiently catalyze the coupling of electron-rich arenes with some alcohols in water.<sup>[8]</sup> Immobilization of lipase enzyme on N-methylglucamine based calix[4]arene magnetic nanoparticles leads to high enantioselectivity, high conversion and fast recovery of product in the hydrolysis reaction of Naproxen methyl ester as compared to encapsulated free enzyme.<sup>[9]</sup> Functionalized CAs are capable to extract metal ions from aqueous and non-aqueous medias due to their cavity size and their substituents affinities to the different types of metal. Acid-amide functionalized CAs were used as ligand to separate uranyl and lanthanides ions from aqueous wastes.<sup>[10]</sup> Metal recognition properties of CAs were studied and revealed that a novel calix[4]arene and bile acid based macrocycle receptor exhibited high binding affinity toward mercury, cadmium, lead, zinc, lithium, manganese and copper metal ions.<sup>[11]</sup> Some functionalized CAs can play an important role as a sensor and exhibit sensing behavior against cations and anions. A novel azocalix[4]arene based sensor has been synthesized and characterized. Experimental studies disclosed that this supramolecular sensor exhibits significant sensing behavior toward  $\text{Cd}^{+2}$  and  $\text{Cu}^{+2}$  among a series of selected transition metals.<sup>[12]</sup> Calix[n]arene capped silver nanoparticles have ability to act as antibacterial agents against Gram positive and Gram negative bacteria,<sup>[13]</sup> endonuclease enzyme inhibitors<sup>[14]</sup> and anti-oxidants.<sup>[15]</sup> The recent straightforward and impressive method for synthesizing organic and inorganic compounds is called Sonochemistry. Sonochemistry is an area of chemistry which is connected with the


[a] R. Eivazzadeh-Keihan, F. Radinekiyan, Prof. A. Maleki  
Catalysts and Organic Synthesis Research Laboratory, Department of Chemistry

Iran University of Science and Technology  
Tehran 16846-13114 (Iran)  
E-mail: maleki@iust.ac.ir

[b] E. B. Noruzi, Dr. B. Shaabani  
Faculty of Chemistry, Department of Inorganic Chemistry  
University of Tabriz  
Tabriz (Iran)  
E-mail: shaabani.b@gmail.com

[c] M. Salimi Bani, Prof. M. Haghpanahi  
School of Mechanical Engineering  
Iran University of Science and Technology  
Tehran, Iran  
E-mail: panahi4m@gmail.com

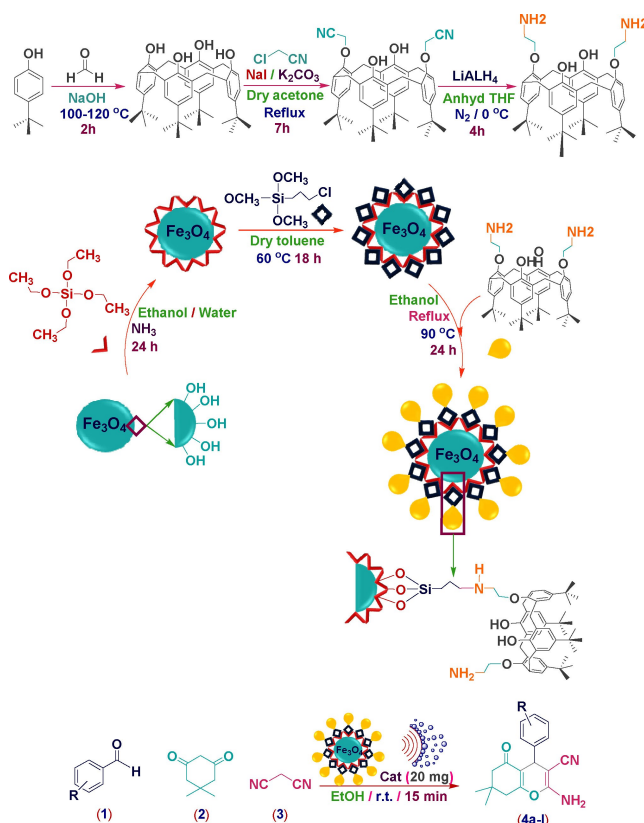
 Supporting information for this article is available on the WWW under <https://doi.org/10.1002/open.202000005>

 © 2020 The Authors. Published by Wiley-VCH Verlag GmbH & Co. KGaA. This is an open access article under the terms of the Creative Commons Attribution Non-Commercial NoDerivs License, which permits use and distribution in any medium, provided the original work is properly cited, the use is non-commercial and no modifications or adaptations are made.

application of high ultrasound energy to the reaction mixture. Ultrasounds are sound waves with high frequencies (greater than 16 KHz). The most important and efficient factor in Sonochemistry is cavitation. The cavitation that is caused by ultrasonic waves, travels through the liquid and accelerates the chemical reactions.<sup>[16]</sup> Cavitation refers to the formation, growth, and implosion of micro-bubbles for short span of time in a liquid. This factor makes extreme high pressures (up to 500 atm), temperatures (up to 5000 °C) and cooling rate (109 °C/s) at the center of the collapsed bubbles which is called hot spots. They activate reactions by supplying the activation energy in the micro environment and enhance the formation of nano-sized structures.<sup>[17]</sup> Energy efficiency, feasible at ambient temperature, enhanced product selectivity, high yield, shorter reaction time, enhanced reaction rates, moderate reaction condition, the formation of non-aggregated products and waste minimization are considerable advantages of ultrasonic-assisted methods compared to other conventional techniques.<sup>[18]</sup> In the last decade, conforming to the multiple capabilities and imperative role of Fe<sub>3</sub>O<sub>4</sub> magnetic nanoparticles (MNPs) in the synthesis of a wide range of Fe<sub>3</sub>O<sub>4</sub>-based nano structural composites, the application of these magnetic nanoparticles have been extended in different scientific fields. On the other hand, the surface of these magnetic nanoparticles is capable of being easily functionalized by applying proper modification methods.<sup>[19]</sup> For instance, a diversity of Fe<sub>3</sub>O<sub>4</sub>-based optical and electrochemical biosensors have been emerged in order to identify cancer toxic proteins,<sup>[20]</sup> cancer biomarkers,<sup>[21]</sup> different mycotoxins<sup>[22]</sup> and pathogenic viruses.<sup>[23]</sup> In other examples, distinctive Fe<sub>3</sub>O<sub>4</sub>-based scaffolds have been applied in tissue engineering with high potent efficiency in attachment, differentiation and cellular proliferation.<sup>[24]</sup> Also, the bio performance of these magnetic nanoparticles with distinctive structures have been approved in *in-vitro* therapeutic hyperthermia therapy.<sup>[25]</sup> In addition, these forefront nanoparticles can be employed as alternative catalytic supports due to their high surface area, outstanding stability, high dispersion and superb catalytic recyclability.<sup>[26]</sup> Conforming to the catalytic activity of Fe<sub>3</sub>O<sub>4</sub>-based nanocomposites in multicomponent reactions,<sup>[27]</sup> in this research, an efficient and functional magnetic nanocomposite based on amino-functionalized calix[4]arenes (MNCACAs) was designed, synthesized and characterized with different spectral and analytical FT-IR, EDX, FE-SEM, TEM, XRD and VSM techniques. Besides, the catalytic efficiency and performance of MNCACAs as a new nano scale catalyst was evaluated in the one-pot three condensation reaction of 2-amino-4*H*-chromene derivatives (Scheme 1).

## 2. Results and Discussion

A new magnetic nanocomposite based on Fe<sub>3</sub>O<sub>4</sub> NPs and their functionalization processes with organic and inorganic molecules was designed and synthesized. The synthetic process of MNCACAs was achieved in five synthetic main steps (Scheme 1). In the first step, 5,11,17,23-Tetra-4-tert-butyl-25,27-di(aminoetboxy)-26,28-dihydroxycalix[4]arene as a last synthetic organic shell was synthe-



**Scheme 1.** Schematic preparation of core-shell MNCACAs and its catalytic activity in one-pot three-components synthesis of 2-amino-4*H*-chromene derivatives.

sized. In the next step, Fe<sub>3</sub>O<sub>4</sub> NPs were synthesized by applying coprecipitation method. Afterwards, the other three synthetic steps which include functionalization processes of synthetic Fe<sub>3</sub>O<sub>4</sub> NPs were carried out by using TEOS and CPTMS inorganic shells and as well synthetic amino-functionalized calix[4]arene as an organic shell. In the following, to determine the characteristics of this novel magnetic nanocomposite, the required spectral and analytical techniques were applied. The generation of new functional groups and also the other main functional groups were conceded with qualitative FT-IR spectra. EDX analysis was used for elemental detection. The size and morphology of designed magnetic nanocomposite were characterized by FE-SEM and TEM images. Eventually, its crystalline phase and magnetic properties were evaluated by XRD pattern and VSM analysis respectively. The characterization of this novel magnetic nanocomposite is discussed in the following.

### 2.1. Evaluation of MNCACAs Characterization

#### 2.1.1. FT-IR analysis

According to qualitative importance of FT-IR analysis in characterization of functional groups, the synthetic process of designed MNCACAs was monitored by this spectroscopic technique (Figure 1a–d). In this respect, Figure 1a shows the FT-

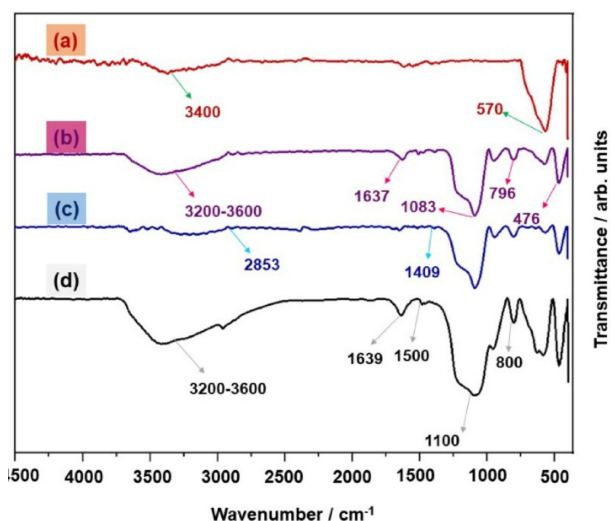


**Figure 1.** FT-IR spectra of (a) unfunctionalized  $\text{Fe}_3\text{O}_4$  NPs, (b)  $\text{Fe}_3\text{O}_4/\text{SiO}_2$ , (c)  $\text{Fe}_3\text{O}_4/\text{SiO}_2/\text{CPTMS}$ , (d) MNCACAs.

IR spectrum of synthetic unfunctionalized  $\text{Fe}_3\text{O}_4$  NPs. As illustrated, the existence of hydroxyl groups on the surface of  $\text{Fe}_3\text{O}_4$  NPs was approved by observing a broad band at a region of  $3400\text{ cm}^{-1}$  which was related to their stretching vibration mode.<sup>[28]</sup> A sharp absorption peak around  $570\text{ cm}^{-1}$  was attributed to Fe–O stretching vibration mode of magnetic phase.<sup>[29]</sup> The first functionalization process of  $\text{Fe}_3\text{O}_4$  NPs by alkoxysilane molecules of TEOS was confirmed by appearance of new absorption bands (Figure 1b). As indicated, the O–H stretching vibration mode was confirmed by observing a broad band in the range of  $3200\text{--}3600\text{ cm}^{-1}$ .<sup>[30]</sup> A small absorption band around  $1637\text{ cm}^{-1}$  were attributed to the O–H stretching vibration mode of Si–OH and twisting vibration mode of adsorbed H–O–H in silica shell. As well as, three absorption peaks near 475 and also around 800 and  $1100\text{ cm}^{-1}$  were determined the existence of bending, symmetric and asymmetric vibration modes of Si–O–Si.<sup>[29–31]</sup> Alongside of mentioned absorption peaks, coating CPTMS molecules on the functionalized surface of  $\text{Fe}_3\text{O}_4$  NPs was characterized due to observing two weak absorption bands around 1409 and  $2855\text{ cm}^{-1}$  which they ascribed to stretching vibration modes of Si–CH<sub>2</sub> and CH<sub>2</sub>. These new absorption bands can concede the interaction accomplishment between CPTMS molecules and coated silica layer.<sup>[32]</sup> Apart from the mentioned absorbance bands, coating the synthetic amino-functionalized calix[4]arene as a third shell on functionalized  $\text{Fe}_3\text{O}_4$  NPs was confirmed by generation of new absorbance bands. As could be seen in Figure 1d, a broad band at the region of  $3200\text{--}3600\text{ cm}^{-1}$  was attributed to the O–H stretching vibration modes which have been covered the N–H stretching modes of primary amine and secondary amine. In comparison of Figure 1c, the intensity of hydroxyl broad absorption band has been increased. According to this observation, it can be concluded that this increment is due to the presence of hydroxyl groups of synthetic amino-functionalized calix[4]arene shell on the functionalized surface of MNPs. The N–H bending vibration modes of primary amine and

secondary amine were characterized by observing two absorbance band around  $1639\text{ cm}^{-1}$  and  $1500\text{ cm}^{-1}$ . The N–H out of plane bending vibration mode was determined due to the presence of an absorbance band at  $802\text{ cm}^{-1}$ . A sharp and almost broad absorbance band around  $1100\text{ cm}^{-1}$  was ascribed to C–N stretching vibration mode of amine which has been overlapped with asymmetric vibration mode of Si–O–Si. As well as, well as, it can be deduced that the absorbance of C=C stretching vibration mode has been covered by N–H bending vibration mode of primary amine.

### 2.1.2. EDX Analysis

As could be seen, the EDX spectrum of designed MNCACAs is indicated in Figure 2. Based on obtained results from EDX analysis, the observed iron peak was related to the synthetic MNPs. The presence of Silicon peak was implied to the functionalization processes of synthetic MNPs and coating  $\text{SiO}_2$  and CPTMS layers on their surface. Two carbon and oxygen peaks can be attributed to the presence of three different TEOS, CPTMS and amino-functionalized calix[4]arenes shells. As well as, the presence of nitrogen peak can be ascribed to the amino groups of synthetic amino-functionalized calix[4]arenes layer. Alongside of mentioned elements, the presence of gold peaks was attributed to the gold sputtering technique of EDX analysis.

### 2.1.3. FE-SEM and TEM Imaging Studies

According to the surface imaging results, the FE-SEM images of MNCACAs is indicated in Figure 3a. As could be observed, the unique structure with sphere morphology and almost uniform distribution was characterized for synthetic MNCACAs. Following the sphere morphology, the formation of core-shell structures was determined due to TEM imaging result (Figure 3b). As well as, the resulted TEM image confirmed that MNPs were well functionalized. Alongside these observations, comforting to the resulted histogram distribution, the average diameter of sphere nanostructures was estimated between 40 to 50 nm (Figure 3c).

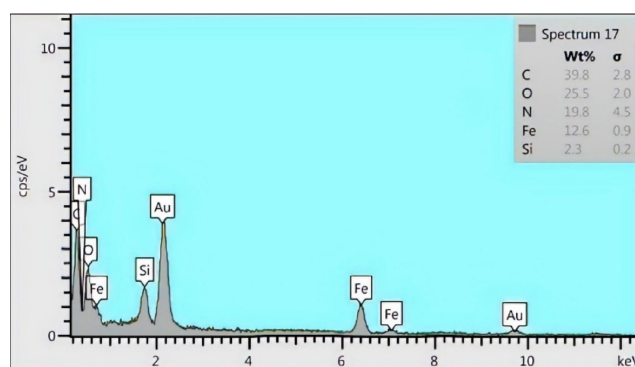


**Figure 2.** EDX spectrum of MNCACAs.

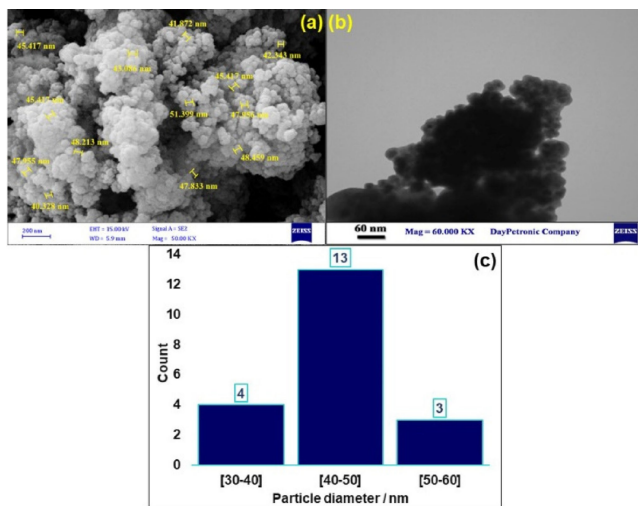


**Figure 3.** (a) FE-SEM image, (b) TEM image of MNCACAs, (c) Histogram of particle size distribution of MNCACAs.

### 2.1.4. XRD Pattern

As could be seen, the XRD pattern of MNCACAs is determined in Figure 4a–b. Based on obtained results from the observed diffraction angles ( $2\theta = 30.25, 35.67, 43.43, 53.65, 57.44, 62.88$ ), the status and intensity of all of the crystalline peaks were complied with the standard XRD pattern of MNPs (JCPDS card No. 01-079-0417).<sup>[33]</sup> Alongside of this compliance, the observed

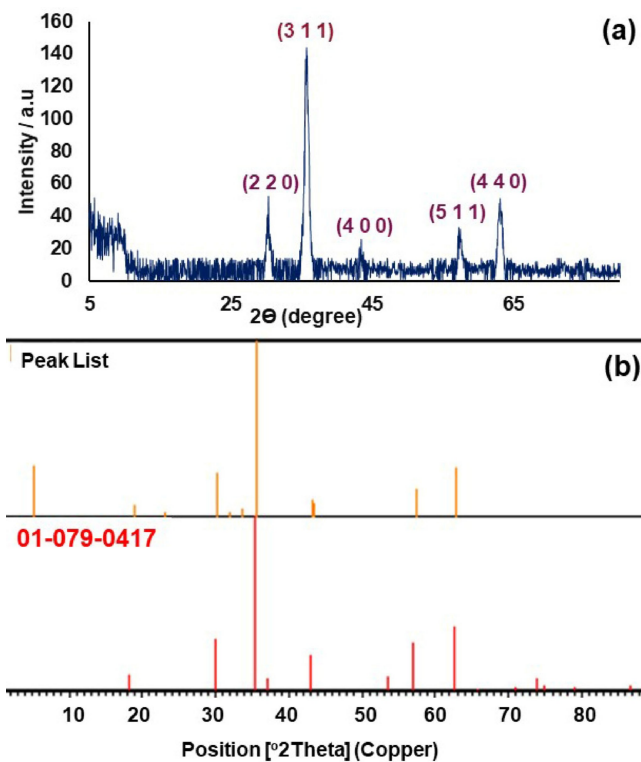


**Figure 4.** (a) XRD pattern of MNCACAs, (b) reference of synthetic MNPs in the structure of MNCACAs

crystalline peaks of MNPs were characterized with their related indices (2 2 0), (3 1 1), (4 0 0), (5 1 1) and (4 4 0).

### 2.1.5. VSM Analysis

In general, saturation magnetization value ( $M_s$ ) of modified and unmodified magnetic nanoparticles are determined by vibrating-sample magnetometer. The hysteresis loop curves of unmodified MNPs and core-shell MNCACAs are indicated in Figure 5a–b. As illustrated, in comparison of unmodified  $\text{Fe}_3\text{O}_4$  MNPs which shows a considerable saturation magnetization value ( $76.20 \text{ emu.g}^{-1}$ ), the saturation magnetization value of MNCACAs has been reduced ( $56.47 \text{ emu.g}^{-1}$ ). According to this reduction, it can be concluded that this reduction is due to functionalization processes and existence of three different coated layers on the surface of  $\text{Fe}_3\text{O}_4$  MNPs.

## 2.2. Evaluation of Catalytic Activity of Core-Shell MNCACAs in Synthesis of 2-Amino-4H-Chromene Derivatives

### 2.2.1. Optimization of Different Parameters in Synthesis of 2-Amino-4H-Chromene Derivatives

In this part, the catalytic performance of MNCACAs was evaluated in synthesis of 2-amino-4H-chromene derivatives. In this regard, in order to optimize the reaction condition, the one-pot three component condensation reaction including

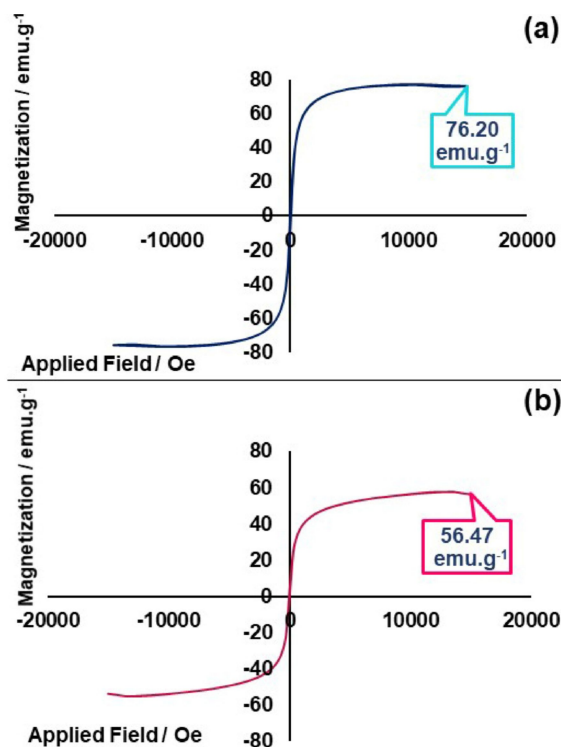


**Figure 5.** Hysteresis loop curves of (a) unmodified  $\text{Fe}_3\text{O}_4$  NPs and (b) MNCACAs.



benzaldehyde (1 mmol), dimedone (1 mmol) and malononitrile (1.5 mmol) was applied as a model reaction. Different parameters including the reaction time, catalyst amount and solvent were investigated to find the optimum reaction condition (Table 1, entries 1–17). Primarily, in the absence of synthetic MNCACAs, the process of model reaction was monitored by using TLC and no specific progression was observed under the room temperature and ultrasonic bath (60 Hz) condition (Table 1, entries 1–2). In the next step, in the presence of 10.00 mg of synthetic magnetic nanocatalyst, the model reaction was examined in two different room temperature and ultrasonic bath (60 Hz) (Table 1, entries 3,6).

As could be observed, due to presence of magnetic nanocatalyst, it can mention that ultrasonic irradiations as a leading factor can move forward the reaction to higher yield percentage of product and shorter reaction time (Table 1, entry 6). Therefore, the ultrasonic bath condition (60 Hz) was determined as an optimized reaction condition. Apart from determining reaction condition, the catalytic impact of each part of designed magnetic nanocatalyst was evaluated. Owing to obtained results from ultrasonic bath reaction condition, in comparison

of equal amount of bare MNPs and synthetic amino-functionalized calix[4]arene (Table 1, entries 4–5), the catalytic activity of MNCACAs disclosed the higher yield percentage of product (84%) in a same reaction time (Table 1, entry 6). Apparently, the functionalization process of modified MNPs by synthetic amino-functionalized calix[4]arene was accompanied with excellent catalytic activity. Apart from catalytic evaluation of designed magnetic nanocomposite, the highest yield percentage of isolated product (93%) was obtained in the presence of 20.00 mg of nanocatalyst (Table 1, entries 6–9) and using ethanol (Table 1, entries 7, 13–17). Alongside of catalyst amount and examining different solvents, it was determined that time increment has not any specific effect in reaction progression and 15 min was considered as optimum reaction time (Table 1, entries 7,10–12).

In order to evaluate the catalytic efficiency of designed MNCACAs, wide range of aromatic aldehydes including electron-withdrawing and electron-releasing substituents (1), dimedone (2), malononitrile (3) were applied to synthesize various 2-amino-4*H*-chromene derivatives (4a–l) under the optimized reaction condition. As summarized in Table 2, the isolated 2-

**Table 1.** Optimization of different parameters due to considering the model reaction.<sup>[a]</sup>

Entry	Catalyst/[mg]	Solvent	Time/[min]	Condition/Temperature/[°C]	Yield <sup>[b]</sup> /[%]
1	–	EtOH	90	r.t./25	N.R
2	–	EtOH	90	Ultrasonic bath/25	N.R
3	MNCACAs 10.00 mg	EtOH	60	r.t./25	66 %
4	Fe <sub>3</sub> O <sub>4</sub> NPs 10.00 mg	EtOH	15	Ultrasonic bath/25	20 %
5	Amino-functionalized calix[4]arene 10.00 mg	EtOH	15	Ultrasonic bath/25	40 %
6	MNCACAs 10.00 mg	EtOH	15	Ultrasonic bath/25	84 %
7	MNCACAs 20.00 mg	EtOH	15	Ultrasonic bath/25	93 %
8	MNCACAs 30.00 mg	EtOH	15	Ultrasonic bath/25	86 %
9	MNCACAs 40.00 mg	EtOH	15	Ultrasonic bath/25	86 %
10	MNCACAs 20.00 mg	EtOH	10	Ultrasonic bath/25	80 %
11	MNCACAs 20.00 mg	EtOH	20	Ultrasonic bath/25	93 %
12	MNCACAs 20.00 mg	EtOH	30	Ultrasonic bath/25	93 %
13	MNCACAs 20.00 mg	Dichloromethane	15	Ultrasonic bath/25	68 %
14	MNCACAs 20.00 mg	acetone	15	Ultrasonic bath/25	66 %
15	MNCACAs 20.00 mg	DMF	15	Ultrasonic bath/25	56 %
16	MNCACAs 20.00 mg	methanol	15	Ultrasonic bath/25	60 %
17	MNCACAs 20.00 mg	Water	15	Ultrasound/25	85 %

[a] The model reaction condition: benzaldehyde (1 mmol), dimedone (1 mmol), malononitrile (1.5 mmol), ethanol (7 mL), ultrasonic bath condition at room temperature (25 °C). [b] Isolated yield.

**Table 2.** Synthesis of 2-amino-4*H*-chromene derivatives by using catalytic performance of MNCACAs.

Entry	Aldehyde	Product	Time/[min]	Yield <sup>[a]</sup> /[%]	Melting point/[°C] Observed	Melting point [°C] Reported
1	benzaldehyde	<b>4a</b>	20	93	228–230	229–231 <sup>[34]</sup>
2	4-methylbenzaldehyde	<b>4b</b>	25	88	218–220	217–219 <sup>[35]</sup>
3	2-methoxybenzaldehyde	<b>4c</b>	25	87	198–200	198–199 <sup>[36]</sup>
4	4-hydroxybenzaldehyde	<b>4d</b>	25	85	206–207	207–208 <sup>[37]</sup>
5	2,4-dihydroxybenzaldehyde	<b>4e</b>	30	85	250–252	249–251 <sup>[38]</sup>
6	2,4-dichlorobenzaldehyde	<b>4f</b>	15	94	209–2011	208–210 <sup>[39]</sup>
7	3-nitrobenzaldehyde	<b>4g</b>	10	95	211–213	211–213 <sup>[40]</sup>
8	2,6-dichlorobenzaldehyde	<b>4h</b>	15	92	249–251	250–252 <sup>[41]</sup>
9	4-chlorobenzaldehyde	<b>4i</b>	18	90	207–209	207–209 <sup>[42]</sup>
10	4-bromobenzaldehyde	<b>4j</b>	20	90	205–207	204–206 <sup>[43]</sup>
11	4-nitrobenzaldehyde	<b>4k</b>	10	92	158–160	157–159 <sup>[38]</sup>
12	4-cyanobenzaldehyde	<b>4l</b>	15	95	227–229	226–228 <sup>[44]</sup>

[a] Isolated yield.

amino-4*H*-chromene derivatives are prepared in high-to-excellent yield percentage (Table 2, entries 1–12).

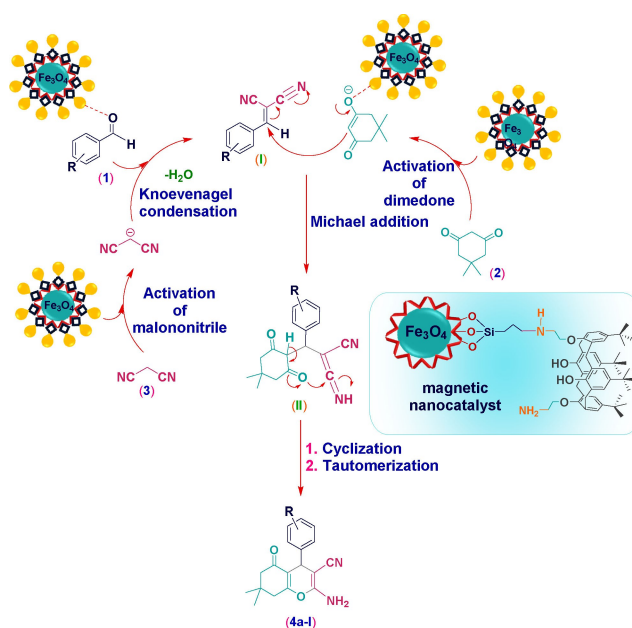
### 2.2.2. Catalytic Evaluation of Designed Magnetic Nanocatalyst Compared to Other Reported Studies

In this part, the catalytic efficiency and performance of designed magnetic nanocatalyst was compared with other homogenous and heterogeneous catalysts which were proposed for the synthesis of 2-amino-4*H*-chromene derivatives. In this regard, the comparison was done based on main parameters such as catalyst amount, time and temperature condition and yield percentage of isolated product.

As illustrated, the comparative results are summarized in Table 3. Due to considering the model reaction which includes benzaldehyde (1 mmol), dimedone (1 mmol) and malononitrile (1.5 mmol), all of the mentioned studies were accompanied with some main problematic factors like using high temperature, reaction accomplishment in a long term interval, low yield percentage of isolated product, catalytic inefficiency of presented catalyst in reaction progression (Table 3, entries 1–6). On the other side, the designed MNCACAs as a new nanocatalyst is accompanied with unique features and specific advantages. Being as a heterogeneous nanocatalyst and owning potential magnetic property prepare a simple separation condition from reaction media. In addition, its considerable catalytic performance in the synthesis of 2-amino-4*H*-chromene derivative (4a) was confirmed via higher yield of the isolated product and shorter reaction time (Table 3, entry 6).

### 2.2.3. Mechanistic Study of Synthetic Magnetic Nanocatalyst in Synthesis of 2-Amino-4*H*-Chromene Derivatives

In this work, the primary amino groups of designed magnetic nanocatalyst are acted as leading and synergic catalytic factors in order to advance the synthesis of 2-amino-4*H*-chromene derivatives. As illustrated, the outline of proposed mechanism is determined in Scheme 2. Conforming to the reported studies in synthesis of 2-amino-4*H*-chromene derivatives,<sup>[49]</sup> in the first step, due to catalytic capability of designed magnetic nanocatalyst in activation, a Knoevenagel condensation reaction between activated malononitrile (3) and activated substituted aldehyde (1) is carried out and the intermediate I is generated.



**Scheme 2.** Plausible mechanism for synthesis of 2-amino-4*H*-chromene derivatives by using MNCACAs.

In the next step, a Michael addition reaction between intermediate I and activated dimedone (2) leads to generation of intermediate II. In the final step which is followed by cyclization and tautomerization reactions, the 2-amino-4*H*-chromene derivatives are formed.

### 2.2.4. Reusability Study of MNCACAs Catalyst

Based on the green chemistry perspectives and significant importance of recovery and recyclability factors in design and fabrication of novel nanocatalyst, the catalytic reusability of MNCACAs was examined in synthesis of 2-amino-4*H*-chromene derivatives. For this purpose, after each reaction completion, the nanocatalyst was simply separated from reaction media due to its considerable magnetic property. Afterwards, the separated nanocatalyst was washed with ethanol solvent and then, for the subsequent catalytic run, it was kept in an oven (80 °C) to dry for an overnight. In the next step, the constant amount of dried nanocatalyst was reused for model reaction. As indicated in Figure 6, without any distinctive reduction in

**Table 3.** Evaluation of catalytic activity of synthetic MNCACAs with other reported studies in synthesis of 2-amino-4*H*-chromene derivatives.<sup>[a]</sup>

Entry	Catalyst	Amount of catalyst/[mg]	Solvent/Temperature condition	Time/[min]	Yield <sup>[b]</sup> /[%]	Reference
1	Fe <sub>3</sub> O <sub>4</sub> @MCM-41@Zr-piperazine-MNPs	30.00 mg	EtOH/H <sub>2</sub> O/75 °C	40	74%	[42]
2	AIL@MNP	60.00 mg	Solvent-free/90 °C	25	89%	[45]
3	Mg(ClO <sub>4</sub> ) <sub>2</sub>	25 w%	EtOH/Reflux	180	90%	[46]
4	RE(POF) <sub>3</sub>	5 mol%	EtOH/60 °C	300	90%	[47]
5	MgO	0.25 g	EtOH/H <sub>2</sub> O/Reflux	30	92%	[48]
6	MNCACAs	20.00 mg	EtOH/Ultrasonic bath (25 °C)	15	93%	Present study

[a] The model reaction conditions: benzaldehyde (1 mmol), dimedone (1 mmol), malononitrile (1.5 mmol), MNCACAs catalyst (20.00 mg), ethanol (7 mL), ultrasonic bath condition at room temperature (25 °C). [b] Isolated yield.

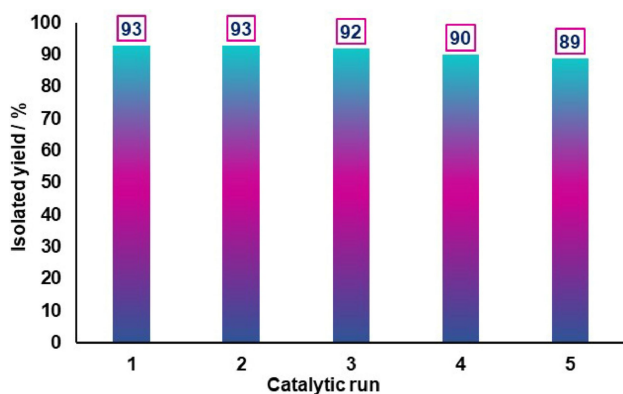


**Figure 6.** Catalytic reusability of synthetic MNCACAs in synthesis of **4a** after 5 catalytic run.

catalytic activity, it was found that the designed magnetic nanocatalyst can be simply recycled at least for five runs.

### 3. Conclusions

In summary, a wide range of heterogeneous magnetic nanocatalysts were designed and synthesized. MNCACAs was introduced as an efficient and functional new nanoscale catalyst for the synthesis of 2-amino-4*H*-chromene derivatives. The evaluation of the structural properties of MNCACAs was carried out by FT-IR, EDX, FE-SEM, TEM, XRD and VSM analysis. The introduction of new functional groups, determination of structural elements, observation of unique morphology spheres, average diameter size (40–50 nm) and core-shell structure and as well as the saturation magnetization value (56.47 emu/g) were carried out. Based on structural features and the compounds characterization, it was disclosed that the notable catalytic efficiency and performance of MNCACAs (20 mg) and the constructive presence of ultrasonic wave irradiations (sonocatalysis) lead to synthesize high yield percentage of the product in a shorter reaction time (15 min).

### Experimental Section

**General:** All the required chemical materials including solvents and reagents were provided from the chemical international companies such as Merck, Fluka and Sigma-Aldrich. The melting points of all solid products were recorded by Electrothermal 9100 apparatus. The ultrasonic bath condition was generated by Elmasonic device (S model, 60 Hz). In order to characterize the formation and presence of new functional groups, the FT-IR spectra were taken by the method of KBr pellets (Shimadzu IR-470 model). <sup>1</sup>H NMR spectrum of amino-functionalized calix[4]arene was characterized by Avance spectrometer (Bruker DRX-500 model) at 400 MHz. The size, morphology and structure of magnetic nanocomposite were determined by field-emission scanning electron microscope (FE-SEM) (ZEISS-sigma VP model) and transmission electron microscope (TEM) (ZEISS-EM10 C-100KV). Energy-dispersive X-ray (EDX) analysis was recorded by Oxford instrument and gold sputtering technique. The XRD pattern of synthetic magnetic nanocomposite was identified by Bruker device (D8 advance model) and also, the

vibrating-sample magnetometer (VSM) analysis was accomplished by LBKFB model-magnetic Kashan kavar (5000 Oe) to measure the saturation magnetization value of designed magnetic nanocomposite. The fabrication process of synthesized magnetic nanocomposite was characterized by obtained results from spectral and analytical data and as well, its catalytic activity was evaluated in synthesis of 2-amino-4*H*-chromene derivatives.

**Preparation of SiO<sub>2</sub> layered Fe<sub>3</sub>O<sub>4</sub> NPs coated by second CPTMS layer (Fe<sub>3</sub>O<sub>4</sub>/SiO<sub>2</sub>-Cl):** The second functionalization process of Fe<sub>3</sub>O<sub>4</sub> NPs by CPTMS molecules was accomplished by the following steps.<sup>[25c]</sup> First, 0.69 g of functionalized Fe<sub>3</sub>O<sub>4</sub> NPs (Fe<sub>3</sub>O<sub>4</sub>/SiO<sub>2</sub>) was mixed with 100 mL of dried toluene at 60 °C under the mechanical stirring condition. After a while, 1 mL of CPTMS solution was added dropwisely to the mixture solution. Then, owing to mentioned thermal reaction condition (60 °C), the suspension solution was kept under the mechanical stirring condition for 18 h. After the mentioned time (18 h), the obtained magnetic product was separated from the reaction media and it was washed with dried toluene for several times. Afterwards, it was kept in a vacuum oven to dry completely.

**Functionalization process of modified Fe<sub>3</sub>O<sub>4</sub> NPs by synthetic amino-functionalized calix[4]arene supramolecules:** In this part, in order to prepare the MNCACAs, first, 1.47 mg of synthetic 5,11,17,23-Tetra-4-tert-butyl-25,27-di(aminoethoxy)-26,28-dihydroxycalix[4]arene was dissolved in a determined amount of ethanol (30 mL). After its complete dissolution, 1.00 g of magnetic chloropropyl-functionalized Fe<sub>3</sub>O<sub>4</sub> NPs was appended to the solution. In the next step, the suspension solution was kept under the reflux condition for 18 h. Due to the reaction completion after the mentioned time, the resulted magnetic product was separated and washed with ethanol for several times. After the elution process, it was dried in the oven at 80 °C for an overnight.

### Competing interest statement

The authors listed in this article have no conflict of interests.

### Acknowledgements

The authors gratefully acknowledge the partial support from the Research Council of the Iran University of Science and Technology.

### Conflict of Interest

The authors declare no conflict of interest.

**Keywords:** 2-amino-4*H*-chromene · calixarenes · heterogeneous catalysis · sonochemistry · supramolecular chemistry

- [1] D. J. Cram, *Angew. Chem.* **1988**, *27*, 1009–1020.
- [2] a) P. E. Goudriaan, P. W. van Leeuwen, M. N. Birkholz, J. N. Reek, *Eur. J. Inorg. Chem.* **2008**, *2008*, 2939–2958; b) P. W. Van Leeuwen, *Supramolecular catalysis*, John Wiley & Sons, vol. **2008**, pp. 1–303.
- [3] a) C. D. Gutsche, J. Stoddart, *Monographs in Supramolecular Chemistry*, Royal Society of Chemistry, Cambridge, **1989**, pp. 210; b) B. Qi, C. Wu, X. Li, D. Wang, L. Sun, B. Chen, W. Liu, H. Zhang, X. Zhou, *ChemCatChem.* **2018**, *10*, 2285–2290.

- [4] P. A. G. P. D. Beer, D. K. Smith, *Supramolecular Chemistry*, Oxford University Press, 1999.
- [5] P. Neri, J. L. Sessler, M.-X. Wang, *Calixarenes and beyond*, Springer, 2016, pp. 1–1057.
- [6] E. BahojbNoruzi, M. Kheirkhahi, B. Shaabani, S. Geremia, N. Hickey, F. Asaro, P. Nitti, H. S. Kafil, *Front. Chem.* 2019, 7, 663.
- [7] a) M. Rahimi, R. Karimian, E. Mostafidi, E. B. Noruzi, S. Taghizadeh, B. Shokouhi, H. S. Kafil, *New J. Chem.* 2018, 42, 13010–13024; b) M. Rahimi, R. Karimian, E. B. Noruzi, K. Ganbarov, M. Zarei, F. S. Kamounah, B. Yousefi, M. Bastami, M. Yousefi, H. S. Kafil, *Int. J. Nanomed.* 2019, 14, 2619–2636.
- [8] S. Sayin, M. Yilmaz, *Tetrahedron* 2014, 70, 6669–6676.
- [9] S. Sayin, E. Yilmaz, M. Yilmaz, *Org. Biomol. Chem.* 2011, 9, 4021–4024.
- [10] P. D. Beer, G. D. Brindley, O. D. Fox, A. Grieve, M. I. Ogden, F. Szemes, M. G. Drew, *J. Chem. Soc. Dalton Trans.* 2002, 3101–3111.
- [11] M. K. Jaiswal, P. K. Muwal, S. Pandey, P. S. Pandey, *Tetrahedron Lett.* 2017, 58, 2153–2156.
- [12] M. A. Qazi, I. Qureshi, S. Memon, *J. Mol. Struct.* 2010, 975, 69–77.
- [13] S. Boudebouze, A. W. Coleman, Y. Tauran, H. Mkaouar, F. Perret, A. Garnier, A. Brioude, B. Kim, E. Maguin, M. Rhimi, *Chem. Commun.* 2013, 49, 7150–7152.
- [14] Y. Tauran, C. Anjard, B. Kim, M. Rhimi, A. Coleman, *Chem. Commun.* 2014, 50, 11404–11406.
- [15] E. Stephens, Y. Tauran, A. Coleman, M. Fitzgerald, *Chem. Commun.* 2015, 51, 851–854.
- [16] G. Chatel, S. Valange, R. Behling, J. C. Colmenares, *ChemCatChem* 2017, 9, 2615–2621.
- [17] a) R. Vinu, G. Madras, *Environ. Sci. Technol.* 2008, 43, 473–479; b) H. Zhao, G. Zhang, Q. Zhang, *Ultrason. Sonochem.* 2014, 21, 991–996; c) J. H. Bang, K. S. Suslick, *Adv. Mater.* 2010, 22, 1039–1059; d) M. Priya, G. Madras, *Ind. Eng. Chem. Res.* 2006, 45, 913–921; e) C. Minero, M. Lucchiarri, D. Vione, V. Maurino, *Environ. Sci. Technol.* 2005, 39, 8936–8942; f) N. G. Khaligh, F. Shirini, *Ultrason. Sonochem.* 2015, 22, 397–403; g) N. C. Eddingsaas, K. S. Suslick, *Nature* 2006, 444, 163–163; h) Y. L. Pang, A. Z. Abdullah, *Ultrason. Sonochem.* 2012, 19, 642–651; i) K. S. Suslick, T. Hyeon, M. Fang, A. A. Cichowlas, *Mater. Sci. Eng. A.* 1995, 204, 186–192; j) A. Ramazani, M. Rouhani, S. W. Joo, *Ultrason. Sonochem.* 2016, 28, 393–399; k) J. Safaei-Ghomi, F. Eshteghal, H. Shahbazi-Alavi, *Ultrason. Sonochem.* 2016, 33, 99–105; l) K. S. Suslick, G. J. Price, *Annual Rev. Mater. Sci.* 1999, 29, 295–326; m) V. Safarifard, A. Morsali, *Coord. Chem. Rev.* 2015, 292, 1–14; n) R. Kuppa, V. S. Moholkar, *Ultrason. Sonochem.* 2010, 17, 123–131; o) Y. T. Didenko, K. S. Suslick, *Nature* 2002, 418, 394–397; p) D. J. Flannigan, K. S. Suslick, *Phys. Rev. Lett.* 2005, 95, 044301; q) H. Flynn, *Phys. Acoust.* 1964, 1, 57–172; r) M. Strasberg, *J. Acoust. Soc. Am.* 1959, 31, 163–176; s) K. Negishi, *J. Phys. Soc. Jpn.* 1961, 16, 1450–1465.
- [18] a) S. K. Saha, P. Chowdhury, P. Saini, S. P. S. Babu, *Appl. Surf. Sci.* 2014, 288, 625–632; b) A. Keramat, R. Zare-Dorabei, *Ultrason. Sonochem.* 2017, 38, 421–429; c) K. Dashtian, R. Zare-Dorabei, *J. Colloid Interface Sci.* 2017, 494, 114–123; d) R. Zare-Dorabei, M. S. Darbandsari, A. Moghimi, M. S. Tehrani, S. Nazerdeylami, *RSC Adv.* 2016, 6, 108477–108487; e) P. De-la-Torre, E. Osorio, J. H. Alzate-Morales, J. Caballero, J. Trilleras, L. Astudillo-Saavedra, I. Brito, A. Cárdenas, J. Quiroga, M. Gutiérrez, *Ultrason. Sonochem.* 2014, 21, 1666–1674; f) D. J. Pacheco, L. Prent, J. Trilleras, J. Quiroga, *Ultrason. Sonochem.* 2013, 20, 1033–1036; g) V. Selvaraj, V. Rajendran, *Ultrason. Sonochem.* 2010, 17, 1236–1244; h) M.-L. Wang, V. Rajendran, *Ultrason. Sonochem.* 2007, 14, 46–54; i) M. Kubo, K. Iimura, T. Yonemoto, *J. Chem. Eng. Jpn.* 2008, 41, 1031–1036; j) Q. Hua, L. Dabin, L. Chunxu, *Ultrason. Sonochem.* 2011, 18, 1035–1037; k) N. Yin, K. Chen, *Polymer* 2004, 45, 3587–3594; l) G. Cravotto, P. Cintas, *Chem. Soc. Rev.* 2006, 35, 180–196; m) B. Sreedhar, P. Surendra Reddy, *Synth. Commun.* 2007, 37, 805–812; n) M. H. Mosslemin, M. R. Nateghi, *Ultrason. Sonochem.* 2010, 17, 162–167.
- [19] a) F. A. Tameh, J. Safaei-Ghomi, M. Mahmoudi-Hashemi, H. Shahbazi-Alavi, *RSC Adv.* 2016, 6, 74802–74811; b) H. Zeng, J. Li, Z. Wang, J. Liu, S. Sun, *Nano Lett.* 2004, 4, 187–190; c) R. Ghosh, L. Pradhan, Y. P. Devi, S. Meena, R. Tewari, A. Kumar, S. Sharma, N. Gajbhiye, R. Vatsa, B. N. Pandey, *J. Mater. Chem.* 2011, 21, 13388–13398.
- [20] R. Eivazzadeh-Keihan, P. Pashazadeh-Panahi, B. Baradaran, M. de la Guardia, M. Hejazi, H. Sohrabi, A. Mokhtarzadeh, A. Maleki, *TrAC Trends Anal. Chem.* 2018, 103, 184–197.
- [21] R. Eivazzadeh-Keihan, P. Pashazadeh-Panahi, B. Baradaran, A. Maleki, M. Hejazi, A. Mokhtarzadeh, M. de la Guardia, *TrAC Trends Anal. Chem.* 2018, 100, 103–115.
- [22] R. Eivazzadeh-Keihan, P. Pashazadeh, M. Hejazi, M. de la Guardia, A. Mokhtarzadeh, *TrAC Trends Anal. Chem.* 2017, 87, 112–128.
- [23] a) A. Mokhtarzadeh, R. Eivazzadeh-Keihan, P. Pashazadeh, M. Hejazi, N. Gharaatifar, M. Hasanzadeh, B. Baradaran, M. de la Guardia, *TrAC Trends Anal. Chem.* 2017, 97, 445–457; b) R. Eivazzadeh-Keihan, P. Pashazadeh-Panahi, T. Mahmoudi, K. K. Chenab, B. Baradaran, M. Hashemzaei, F. Radinekiyan, A. Mokhtarzadeh, A. Maleki, *Microchim. Acta.* 2019, 186, 329.
- [24] R. Eivazzadeh-Keihan, A. Maleki, M. de la Guardia, M. S. Bani, K. K. Chenab, P. Pashazadeh-Panahi, B. Baradaran, A. Mokhtarzadeh, M. R. Hamblin, *J. Adv. Res.* 2019, 18, 185–201.
- [25] a) M. S. Bani, S. Hatamie, M. Haghpahan, H. Bahreinizad, M. H. S. Alavijeh, R. Eivazzadeh-Keihan, Z. H. Wei, *Spin.* 2019, 9; b) R. Eivazzadeh-Keihan, F. Radinekiyan, A. Maleki, M. S. Bani, Z. Hajizadeh, S. Asgharnasl, *Int. J. Biol. Macromol.* 2019, 140, 407–414; c) R. Eivazzadeh-Keihan, F. Radinekiyan, A. Maleki, M. S. Bani, M. Azizi, *J. Mater. Sci.* 2020, 55, 319–336.
- [26] Y. Zhu, L. P. Stubbs, F. Ho, R. Liu, C. P. Ship, J. A. Maguire, N. S. Hosmane, *ChemCatChem* 2010, 2, 365–374.
- [27] a) A. Maleki, S. Azadegan, *Inorg. Nano. Metal. Chem.* 2017, 47, 917–924; b) A. Maleki, H. Movahed, P. Ravaghi, *Carbohydr. Polym.* 2017, 156, 259–267.
- [28] L. Ji, L. Zhou, X. Bai, Y. Shao, G. Zhao, Y. Qu, C. Wang, Y. Li, *J. Mater. Chem.* 2012, 22, 15853–15862.
- [29] S. Villa, P. Riani, F. Locardi, F. Canepa, *Materials* 2016, 9, 826.
- [30] M. Safaiee, M. A. Zolfigol, F. Afsharnadery, S. Baghery, *RSC Adv.* 2015, 5, 102340–102349.
- [31] M. Farahi, B. Karami, R. Keshavarz, F. Khosravian, *RSC Adv.* 2017, 7, 46644–46650.
- [32] E. G. Vieira, I. V. Soares, N. C. Da Silva, S. D. Perujo, D. R. Do Carmo, N. L. Dias Filho, *New J. Chem.* 2013, 37, 1933–1943.
- [33] H. El Ghandoor, H. Zidan, M. M. Khalil, M. Ismail, *Int. J. Electrochem. Sci.* 2012, 7, 5734–5745.
- [34] M. A. Bodaghifard, M. Hamidinasab, N. Ahadi, *Curr. Org. Chem.* 2018, 22, 234–267.
- [35] H. R. Saadati-Moshtaghin, F. M. Zonoz, *Inorg. Chem. Commun.* 2018, 99, 44–51.
- [36] D. Tahmassebi, J. A. Bryson, S. I. Binz, *Synth. Commun.* 2011, 41, 2701–2711.
- [37] X. Xiong, C. Yi, X. Liao, S. Lai, *Catal. Lett.* 2019, 149, 1690–1700.
- [38] M. A. Zolfigol, N. Bahrami-Nejad, F. Afsharnadery, S. Baghery, *J. Mol. Liq.* 2016, 221, 851–859.
- [39] R. Ramesh, P. Vadivel, S. Maheswari, A. Lalitha, *Res. Chem. Intermed.* 2016, 42, 7625–7636.
- [40] M. Haghighat, F. Shirini, M. Golshekan, *J. Nanosci. Nanotechnol.* 2019, 19, 3447–3458.
- [41] A. Khazaei, F. Gholami, V. Khakyzadeh, A. R. Moosavi-Zare, J. Afsar, *RSC Adv.* 2015, 5, 14305–14310.
- [42] R. Pourhasan-Kisomi, F. Shirini, M. Golshekan, *Appl. Organomet. Chem.* 2018, 32, e4371.
- [43] J. M. Khurana, B. Nand, P. Saluja, *J. Heterocycl. Chem.* 2014, 51, 618–624.
- [44] E. Abbaspour-Gilandeh, M. Aghaei-Hashjin, A. Yahyazadeh, H. Salemi, *RSC Adv.* 2016, 6, 55444–55462.
- [45] Q. Zhang, Y.-H. Gao, S.-L. Qin, H.-X. Wei, *Catalysts* 2017, 7, 351.
- [46] M. M. Zeydi, S. Ahmadi, *Orient. J. Chem.* 2016, 32, 2215.
- [47] L.-M. Wang, J.-H. Shao, H. Tian, Y.-H. Wang, B. Liu, *J. Fluorine Chem.* 2006, 127, 97–100.
- [48] M. Seifi, H. Sheibani, *Catal. Lett.* 2008, 126, 275–279.
- [49] I. A. Azath, P. Puthiaraj, K. Pitchumani, *ACS Sustainable Chem. Eng.* 2012, 1, 174–179.

Manuscript received: January 11, 2020

Revised manuscript received: March 1, 2020